Numerical Investigation of Die Geometry Effect on LDPE Annular Extrudate Swell

Y. Mu,[1,2,3] Guoqun Zhao,[1,2] Chengrui Zhang[3]

[1]*Key Laboratory for Liquid-Solid Structural Evolution and Processing of Materials (Ministry of Education), Shandong University, Jinan, Shandong 250061, People's Republic of China*
[2]*Engineering Research Center for Mould and Die Technologies, Shandong University, Jinan, Shandong 250061, People's Republic of China*
[3]*School of Mechanical Engineering, Shandong University, Jinan, Shandong 250061, People's Republic of China*

Received 21 April 2009; accepted 22 September 2009
DOI 10.1002/app.31490
Published online 2 March 2010 in Wiley InterScience (www.interscience.wiley.com).

ABSTRACT: Extrudate swell is a common phenomenon in the polymer processing. The investigation of its mechanism has both scientific and industrial interest. In the study, the swell phenomenon of LDPE flowing through annular extrusion die is investigated by using finite element simulation. The effects of die geometry on the annular extrudate swell and on the polymer flow patterns are discussed in detail. The rheology of LDPE is described by using viscoelastic PTT (Phan-Thien-Tanner) constitutive model and the corresponding material parameters are obtained by fitting the material functions detected on a strain-controlled rheometer. The mathematical model of annular extrudate swell is established and its finite element model is derived in the study. A penalty method is employed to solve the extrudate swell problem with a decoupled algorithm. The computation stability is improved by using the discrete elastic-viscous split stress (DEVSS) algorithm with the inconsistent streamline-upwind (SU) scheme. The essential flow characteristics of polymer melts flowing through annular extrusion die with different die contraction angles, different ratios of parallel length to inner radius, and different ratios of outer to inner radius are then predicted by using the proposed numerical method and the mechanism of swell phenomenon is further discussed. © 2010 Wiley Periodicals, Inc. J Appl Polym Sci 117: 91–109, 2010

Key words: polymer; extrudate swell; die geometry; viscoelastic; finite element simulation

INTRODUCTION

Annular flow is a common flow pattern in polymer processing, such as blow molding, pipe extrusion, and wire coating. When polymer melts are extruded through out of the flow channel without any traction force, the dimension of extrudate cross section will be larger than that of the flow channel outlet. Such unique phenomenon is usually called extrudate swell or barus effect that is greatly determined by the flow pattern of polymer melts within the mold/die.

Many researchers have dedicated to explain this unique phenomenon. Lodge[1] firstly proposed a theory of elastic recovery. Tanner[2] presented an elastic-fluid theory for die-swell in the long dies. Nickell et al.[3] implemented various finite element methods for creeping die-swell Newtonian flows. Chang et al.[4] applied collocation and Galerkin methods to the slit and circular die swell flows for a generalized Maxwell fluid. Caswell and Viriyayuthakorn[5] presented Newtonian and viscoelastic finite element formulations with a classical displacement method. Bush et al.[6] presented planar and axisymmetric extrusion flow analyses using both finite element and boundary integral methods for Maxwell fluids which involved the computation along streamlines.

Numerical simulation as a highly effective method can well predict such complex phenomenon and hence to explain relevant mechanism. However, most of recent researches are still aiming at solving supposed or simplified numerical examples including the hypothesis of material parameters and flow domain characteristics. It can be acceptable for the establishment or training of numerical algorithm. However, from an industrial viewpoint, a more rigorous model for practical flow problem is necessary to capture the whole flow patterns.

In this study, the rheological behavior of a typical engineering material LDPE flowing through out of annular extrusion die is investigated by using numerical simulation and hence to explain the swell

Correspondence to: Y. Mu (ymu@sdu.edu.cn) or G. Zhao (zhaogq@sdu.edu.cn).
Contract grant sponsor: National Natural Science Foundation for Distinguished Young Scholars of China; contract grant number: 50425517.

TABLE I
Relaxation Spectrum

i	λ_i (s)	g_i(Pa)	η_i (Pa s)
1	0.001383	1575179.77	2178.47
2	0.012416	283022.03	3514.00
3	0.051122	135446.08	6924.27
4	0.214309	69492.85	14892.94
5	1.078078	30431.42	32807.44
6	8.095599	9105.95	73718.11

mechanism. The effects of die geometry on both polymer melts flow patterns and annular extrudate swell are predicted and discussed in detail. The viscoelastic flow properties are described by a differential PTT (Phan-Thien-Tanner) constitutive model[7] whose rheological parameters are obtained by fitting the distributions of material function detected on a strain-controlled rheometer. The mathematical model of three-dimensional (3D) annular extrudate swell of viscoelastic fluid is established. The finite element simulation of extrudate swell is performed and the details of numerical schemes adopted are presented. The penalty finite element method and a decoupled solving method are implemented to reduce the computation memory requirement. The discrete elastic-viscous split stress (DEVSS) algorithm incorporating the inconsistent streamline-upwind (SU) scheme is employed to improve the computation stability. The ellipticity of the momentum equation is improved by the addition of a stabilization factor and the influence of convection term in the constitutive equation is controlled by an asymmetric weighting function. The outlet free surface of extrudate is determined by using the criterion of no mass penetration across the free surface and it is adjusted by a streamface-streamline method.[8] The essential flow characteristics of polymer melts flowing through out of annular extrusion die are further investigated by using the established mathematical model and solution algorithm. The effects of die parameters including the die contraction angle, the ratio of parallel length to inner radius, and the ratio of outer to inner radius on the LDPE annular extrudate swell are discussed in detail.

MATERIAL CHARACTERIZATION

The material investigated in the study is a commercial low density polyethylene (LDPE) whose density and melt index are, respectively, 0.9292 g/cm^3 and 2.2 g/10 min. An exponential PTT (Phan-Thien-Tanner) constitutive model is used to capture its viscoelastic rheological properties. The model parameters are obtained by fitting the distributions of material function detected on a strain-control rheometer.

The samples of the tested material are firstly prepared by compression molding pellets at 180°C. The diameter and the thickness of the samples are, respectively, 25 mm and 2 mm. The variations of storage modulus G' and loss modulus G'' versus angular frequency ω are firstly obtained in experimental flow with small amplitued shear oscillation. The variations of viscosity η and the first normal stress difference N_1 versus shear rate $\dot{\gamma}$ in steady shear flow are then detected on the rheometer.

In linear viscoelastic flow region, the storage modulus and the loss modulus can be written as the function of angular frequency as follows:

$$G'(\omega) = \sum_{i=1}^{n} \frac{g_i \lambda_i^2 \omega^2}{1 + \lambda_i^2 \omega^2}, \quad G''(\omega) = \sum_{i=1}^{n} \frac{g_i \lambda_i \omega}{1 + \lambda_i^2 \omega^2} \tag{1}$$

where g_i is the shear elastic modulus, λ_i is the discrete relaxation time, and n is the number of relaxation mode.

Both g_i and λ_i are important linear viscoelastic parameters. According to the nonlinear regression method, a six-mode relaxation time spectrum as show in Table 1 is obtained by fitting the experimental results of storage modulus and loss modulus as shown in Figure 1.

A single mode relaxation time is adopted in the study and the average relaxation time $\overline{\lambda} = 5.743$ s is derived as follows:

$$\overline{\lambda} = \sum_{i=1}^{n} \lambda_i g_i \lambda_i \Big/ \sum_{i=1}^{n} g_i \lambda_i \tag{2}$$

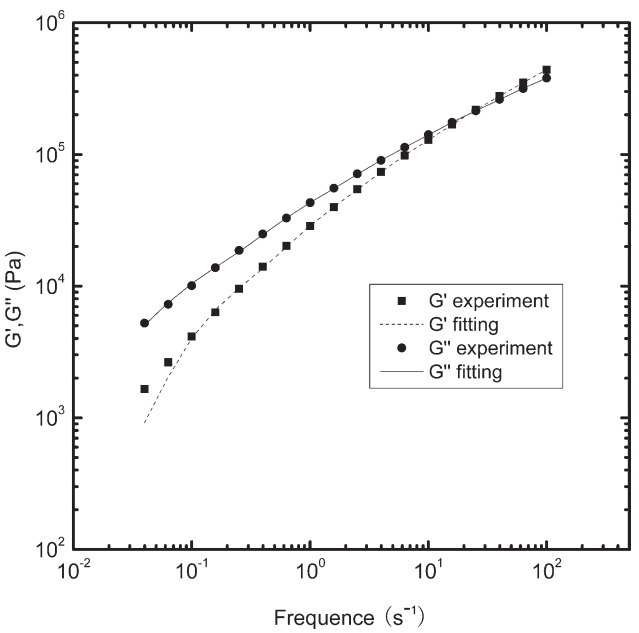

Figure 1 Fitting of linear viscoelastic parameters (180°C).

As for the PTT viscoelastic model, the material functions of viscosity η and the first normal stress difference N_1 in steady shear flow can be, respectively, written as the following function of shear rate $\dot{\gamma}$

$$\eta(\dot{\gamma}) = \sum_{i=1}^{n} \frac{f_i \eta_i}{f_i^2 + \xi(2-\xi)(\lambda_i \dot{\gamma})^2} \tag{3}$$

$$N_1(\dot{\gamma}) = \sum_{i=1}^{n} \frac{2\eta_i \lambda_i \gamma_i^2}{f_i^2 + \xi(2-\xi)(\lambda_i \dot{\gamma})^2} \tag{4}$$

where the coefficient f_i obeys the following:

$$\left\{ f_i^2 + \xi(2-\xi)(\lambda_i \dot{\gamma})^2 \right\} \ln f_i = 2\varepsilon(1-\xi)(\lambda_i \dot{\gamma})^2 \tag{5}$$

Two nonlinear viscoelastic parameters $\varepsilon = 0.0836$ and $\xi = 0.0145$ can be obtained by fitting experimental results according to nonlinear regression method as shown in Figure 2, where ε is a parameter limiting the extensional viscosity of the fluid and ξ is the slip parameter related to the second normal stress difference.[9]

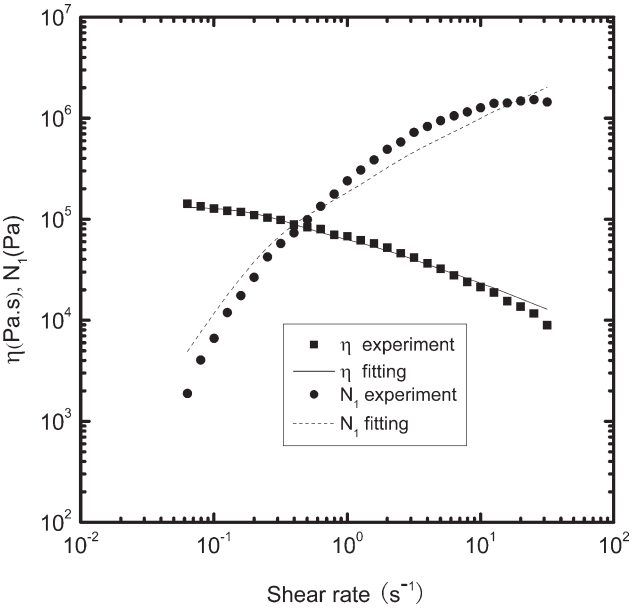

Figure 2 Fitting of nonlinear viscoelastic parameters (180°C).

MATHEMATICAL MODELING

Governing equations

According to the theory of Computational Fluid Dynamics, the governing equations to solve the fluids flow problems can be obtained from the continuity equation, momentum equation, and energy equation, respectively, based on the conservation of mass, momentum, and energy.[10] Considering the characteristics of polymer melts flow in the die channel when a successive extrusion is arrived, the hypothesis of isothermal incompressible steady laminar flow is made in the study. The governing equations for the viscoelastic flow of polymer melts obeying PTT model take the following form:

$$\text{Continuity equation} \quad \nabla \cdot u = 0 \tag{6}$$

$$\text{Momentum equation} \quad \nabla \cdot S - \nabla p = 0 \tag{7}$$

$$\text{Constitutive equation} \quad S = 2\eta_v d + \tau \tag{8}$$

where $\bigtriangledown$ is the Hamilton differential operator, u is the velocity vector, p is the hydrostatic pressure, S is the extra stress tensor, η_v is the newtonian-contribution viscosity, τ is the polymer-contribution stress, and d is the strain rate tensor which obeys the following:

$$d = (\nabla u + \nabla u^T)/2 \tag{9}$$

By introducing the retardation ratio β, defined as follows:

$$\beta = \frac{\eta_p}{\eta_t} \tag{10}$$

where $\eta_t = \eta_p + \eta_v$ is the total viscosity and η_p is the polymer-contribution viscosity. As for the flow of polymer melts in the extrusion process, the Newtonian-contribution viscosity η_v is far less than the polymer-contribution viscosity η_p ($\eta_v \ll \eta_p$) and hence $\beta = 1.0$ is adopted in the study.

The polymer-contribution stress τ obeys the following equation:

$$\lambda \overline{\tau} + g(\tau)\tau = 2\beta\eta_t d \tag{11}$$

where λ is the relaxation time and $g(\tau)$ is a stress function following the exponential form proposed in the original work of Phan-Thien and Tanner

$$g(\tau) = \exp\left(\frac{\lambda\varepsilon}{\beta\eta_t} tr(\tau)\right) \tag{12}$$

The full PTT constitutive model based on Gordon-Schowalter (GS) convected derivative is adopted and τ denotes the following Gordon-Schowalter convected derivative operator[11]

$$\overline{\tau} = \frac{\partial \tau}{\partial t} + u \cdot \nabla\tau - (\nabla u - \xi d) \cdot \tau - \tau \cdot (\nabla u - \xi d)^T \tag{13}$$

Equation (13) can be simplified into the upper convective derivative when the parameter ξ of the GS derivative is set to zero.

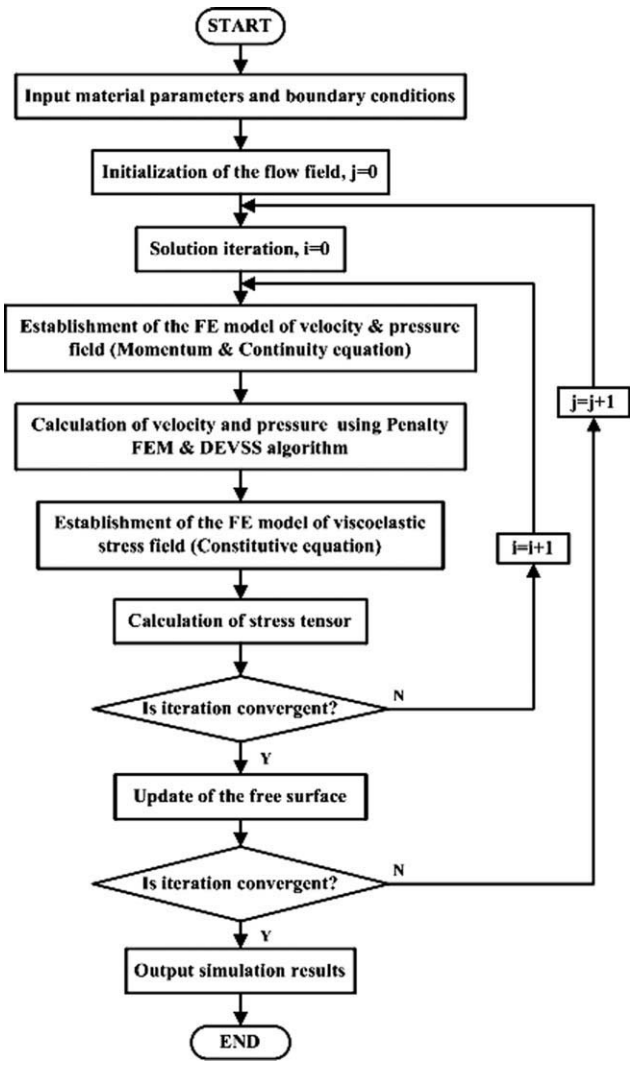

Figure 3 Flow chart of the finite element simulation.

Solution method

A decoupled iteration method as shown in Figure 3 is employed to solve the swell problem of viscoelastic fluid.[12] The location of the free surface as part of the unknowns in the swell problem is firstly assumed and initialized. The finite element simulation is then performed for the calculation of each field variable in the current viscoelastic flow field.

The penalty finite element algorithm[13] is employed to solve the nonlinear system consisting of the continuity equation and momentum equation. The penalty factor as a function obeying $\lambda_p = \frac{p}{\nabla \cdot u}$ is firstly introduced to avoid a direct calculation of the hydrostatic pressure and hence to reduce the computation memory requirement. The following relationship is thereby obtained as follows:

$$p = -\lambda_p \nabla \cdot u \tag{14}$$

Substituting eqs. (8), (10), and (14) into the momentum eq. (7), the following momentum governing equation can be obtained:

$$\nabla(\lambda_p \nabla \cdot u) + 2(1-\beta)\eta_t \nabla \cdot d + \nabla \cdot \tau = 0 \tag{15}$$

To improve the convergence property of the numerical scheme, the DEVSS (discrete elastic-viscous split stress) formulation[14] is adopted and an ellipticity factor $2\overline{\eta}[\Sigma(u) - d]$ is introduced into the momentum equation eq. (15). The following equation is obtained:

$$2\overline{\eta}\nabla \cdot \Sigma(u) + \lambda_p \nabla(\nabla \cdot u) = 2(\overline{\eta} - (1-\beta)\eta_t)\nabla \cdot d - \nabla \cdot \tau \tag{16}$$

where $\Sigma(u) = (\bigtriangledown u + \bigtriangledown^T u)/2$, $\overline{\eta}$ is a reference viscosity.

The velocity vector is firstly solved from eq. (16) by treating the polymer-contribution stress tensor and the strain rate tensor as known terms

$$2\overline{\eta}\nabla \cdot \Sigma(u^i) + \lambda_p \nabla(\nabla \cdot u^i) = 2(\overline{\eta} - (1-\beta)\eta_t)\nabla \cdot d^{i-1} - \nabla \cdot \tau^{i-1} \tag{17}$$

where d^{i-1} and τ^{i-1} are, respectively, the strain rate tensor and the stress tensor calculated with the flow field at the previous iteration step $i-1$ and their initial values are derived from a viscous flow field, i is the current iteration step of flow field calculation.

The polymer-contribution stress tensor is thereafter calculated through the constitutive equation eq. (18) based on the velocity solution obtained from the calculation of the momentum equation eq. (17).

$$\lambda\left(u^i \cdot \nabla\tau^i - (\nabla u^i)\cdot\tau^i - \tau^i \cdot (\nabla u^i)^T + \frac{\xi}{2}\left(\left(\nabla u^i + (\nabla u^i)^T\right)\cdot\tau^i + \tau^i \cdot \left(\nabla u^i + (\nabla u^i)^T\right)\right)\right) + \left(\exp\left(\frac{\lambda\varepsilon}{\beta\eta_t} tr(\tau^{i-1})\right)\right)\tau^i = \beta\eta_t\left(\nabla u^i + (\nabla u^i)^T\right) \tag{18}$$

where the nonlinear term is derived from the stress tensor obtained from last iteration step $i-1$.

The convergent criteria of calculation in the current flow field are defined upon the following requirements as eq. (19). When the relative error of each variable is less than a set value, convergence is considered to be achieved.

$$\left|\frac{\sum(u^i - u^{i-1})}{\sum u^i}\right| < \delta_u, \quad \left|\frac{\sum(\tau^i - \tau^{i-1})}{\sum \tau^i}\right| < \delta_\tau \tag{19}$$

where δ_u is the convergent criterion of the velocity vector which is set to 10^{-4} here and δ_τ is the convergent criterion of the polymer-contribution stress tensor which is set to 10^{-3} in the study.

In the process of extrudate swell simulation, the velocity boundary condition is treated as a criterion to adjust the location of free surface and only the force boundary condition is imposed on the free surface. When a convergent solution in the current flow field is achieved, the location of free surface can be determined by using the criterion of no mass penetration across the free surface or that the normal velocity on the free surface is zero.

The swelling free surface as show in Figure 4 is a stream surface which can be expressed as follows:

$$\frac{dx}{u_x} = \frac{dy}{u_y} = \frac{dz}{u_z} \tag{20}$$

After integration, the following equation to calculate the free surface is obtained:

$$x_b = x_a + \int_{z_a}^{z_b} \frac{u_x}{u_z} dz, \qquad y_b = y_a + \int_{z_a}^{z_b} \frac{u_y}{u_z} dz \tag{21}$$

The location of the free surface can then be adjusted according to the eq. (21). The finite element simulation is thereafter conducted in the current adjusted flow field. The process is repeated until the maximum coordinate difference between two iteration steps is less than the tolerance defined as below

$$\max\left(\left|\frac{x^j - x^{j-1}}{x^{j-1}}\right|\right) < \delta_x, \qquad \max\left(\left|\frac{y^j - y^{j-1}}{y^{j-1}}\right|\right) < \delta_y \tag{22}$$

where δ_x and δ_y are, respectively, the permissible coordinate difference of x and y coordinate values which are both set to 0.005 in the study, j is the current iteration step of coordinate.

Finite element formulations

The Galerkin weighting residual method is adopted for the discretization of the momentum equation where the weighting function is taken as the same form as the interpretation function. The discretized momentum equation at the elemental level is expressed as follows:

$$\int_{\Omega^e} N(2\overline{\eta}\nabla \cdot \Sigma(u) + \lambda_p \nabla(\nabla \cdot u)) d\Omega = \int_{\Omega^e} N(2(\overline{\eta} - (1-\beta)\eta_t)\nabla \cdot d - \nabla \cdot \tau) d\Omega \tag{23}$$

After Green-Gauss transformation, the following weak form of eq. (23) can be obtained:

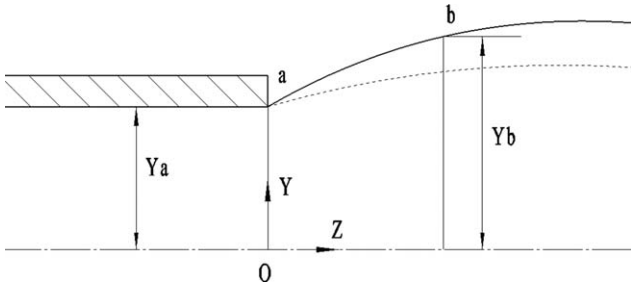

Figure 4 Update of the free surface.

$$\int_{\Omega^e} \nabla N(\overline{\eta}(\nabla u + \nabla u^T) + \lambda_p(\nabla \cdot u)) d\Omega = \int_{\Omega^e} \nabla N(2(\overline{\eta} - (1-\beta)\eta_t)d - \tau) d\Omega + \int_{S^e} N^*(\tau - p) \cdot n dS \tag{24}$$

where N^* is equal to the interpolation function on the boundary force, Ω^e and S^e are, respectively, the element region and element boundary, and n is the outer normal unit vector.

The discretized momentum eq. (24) is then developed in three vector components (x, y, and z directions) and the following elemental stiffness matrix equation is obtained.

$$\begin{bmatrix} K_{ij}^{11} & K_{ij}^{12} & K_{ij}^{13} \\ K_{ij}^{21} & K_{ij}^{22} & K_{ij}^{23} \\ K_{ij}^{31} & K_{ij}^{32} & K_{ij}^{33} \end{bmatrix} \begin{Bmatrix} u_j^x \\ u_j^y \\ u_j^z \end{Bmatrix} = \begin{Bmatrix} F_i^x \\ F_i^y \\ F_i^z \end{Bmatrix} \quad (i,j = 1,2,\cdots,8) \tag{25}$$

According to the nodes superposition principle and element connectivity, the global stiffness matrix equation of the motion equation eq. (26) for all the elements can be assembled after evaluating the elemental stiffness matrix at elemental level using eq. (25).

$$K_{nm} u_m = F_n, \ (m = n = 3 \times M) \tag{26}$$

where K_{nm} is the global stiffness matrix of the momentum equation, u_m is all the nodal velocity components, F_n corresponds to the equation residuals, and M is equal to the number of finite element nodes.

The velocity solution will be obtained by solving the eq. (26) after the boundary condition being introduced. Based on the velocity solution, solutions of pressure p and the strain rate tensor d can be, respectively, derived from eqs. (14) and (9).

As for the discretization of the constitutive equation, the effect of convective term $u \cdot \bigtriangledown\tau$ should be well considered. When the convective term becomes dominant as the Weissenberg number increased, the classical Galerkin weighting residual method will lose its optimal approximation. The inconsistent

streamline-upwind (SU) method is adopted here to control the convective effect and an asymmetric weighting function W_i is introduced.

$$W_i = N_i + \frac{\bar{k}u}{(u \cdot u)} \cdot \nabla N_i, \ (i = 1, 2, ..., 8) \tag{27}$$

where N_i is equal to the classical Galerkin weighting function, the coefficient $\bar{k}$ is defined by the velocity components at the element center u_ξ, u_η, u_ζ as proposed by Marchal and Crochet.[15]

$$\bar{k} = (u_\xi^2 + u_\eta^2 + u_\zeta^2)^{1/2}/2 \tag{28}$$

The additional term of the weighting function $\frac{\bar{k}u}{(u \cdot u)} \cdot \nabla N_i$ is only imposed on the purely advective term $u \cdot \bigtriangledown\tau$ in the constitutive eq. (18) and the following elemental constitutive equation is obtained.

$$\begin{aligned}\int_{\Omega^e} N_i \Big(\lambda\Big(&- (\nabla u) \cdot \tau - \tau \cdot (\nabla u)^T + \xi\Big(\Big(\nabla u + (\nabla u)^T\Big) \\ &\cdot \tau + \tau \cdot \Big(\nabla u + (\nabla u)^T\Big)\Big)\Big)\Big) d\Omega + \int_{\Omega^e} W_i(\lambda(u \cdot \nabla\tau)) d\Omega \\ &+ \int_{\Omega^e} N_i \Big(\Big(1 + \frac{\lambda\varepsilon}{\beta\eta_t} tr(\tau)\Big)\tau\Big) d\Omega \\ &= \int_{\Omega^e} N_i \Big(\beta\eta_t \Big(\nabla u + (\nabla u)^T\Big)\Big) d\Omega \end{aligned} \tag{29}$$

Equation (29) is then developed in three vector components directions and the elemental stiffness matrix equation is obtained as follows:

$$\begin{bmatrix} K_{ij}^{11} & K_{ij}^{12} & K_{ij}^{13} & 0 & 0 & 0 \\ K_{ij}^{21} & K_{ij}^{22} & K_{ij}^{23} & K_{ij}^{24} & K_{ij}^{25} & 0 \\ K_{ij}^{31} & K_{ij}^{32} & K_{ij}^{33} & 0 & K_{ij}^{35} & K_{ij}^{36} \\ 0 & K_{ij}^{42} & 0 & K_{ij}^{44} & K_{ij}^{45} & 0 \\ 0 & K_{ij}^{52} & K_{ij}^{53} & K_{ij}^{54} & K_{ij}^{55} & K_{ij}^{56} \\ 0 & 0 & K_{ij}^{63} & 0 & K_{ij}^{65} & K_{ij}^{66} \end{bmatrix} \begin{Bmatrix} \tau_j^{xx} \\ \tau_j^{xy} \\ \tau_j^{xz} \\ \tau_j^{yy} \\ \tau_j^{yz} \\ \tau_j^{zz} \end{Bmatrix} = \begin{Bmatrix} F_i^1 \\ F_i^2 \\ F_i^3 \\ F_i^4 \\ F_i^5 \\ F_i^6 \end{Bmatrix} (i, j = 1, 2, \cdots, 8) \tag{30}$$

The global stiffness matrix equation of the constitutive equation eq. (31) for all the elements is assembled after the elemental calculation according to the nodes superposition principle. The extra stress tensor can be obtained by solving the global stiffness matrix equation of the constitutive equation eq. (31) using a direct calculation algorithm.

$$K_{nm}\tau_m = F_n, \ (m = n = 6 \times M) \tag{31}$$

where K_{nm} is the global stiffness matrix of the constitutive equation, τ_m is all the nodal stress components, F_n corresponds to the equation residuals, and M is equal to the number of finite element nodes.

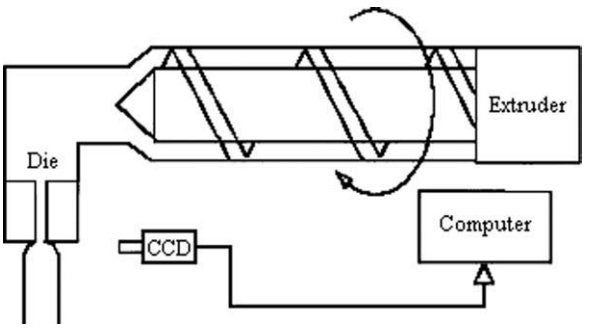

Figure 5 Schematic diagram of experimental apparatus.

Experimental verification

To verify the rationality of the proposed mathematical model and numerical method, the simulated swell ratio of LDPE flowing through a circular die is compared with that of the corresponding experimentally measured results. The experimental measurement is conducted on a Haake rheometer which is a kind of torque rheometer with multifunction to study melts flow behaviors in polymer processing. When being equipped with a screw, the rheometer can be considered as a small size extruder. The Haake rheometer equipped with a circular die of 2 mm diameter whose length to diameter ratio is 30 : 1 as shown in Figure 5 is adopted in the study to simulate practical extrusion process of LDPE as that in the extruder. A CCD camera is fixed out of the die lip and the swell phenomenon of LDPE is photographed at real time as shown in Figure 6.

A 3D simulation is conducted to predict the swell phenomenon of LDPE flowing through out of the circular die as depicted in the experimental measurement. Material parameters obtained in the rheological test as shown in "Material Characterization" are adopted in the numerical calculation to describe the viscoelastic properties of LDPE. The melts flow in one-quarter of the symmetrical flow channel is analyzed and the solved domain is divided into trilinear brick elements by means of mapping mesh generation technology as shown in Figure 7. There is strong singularity near the die lip where the boundary condition has a sudden variation from nonslip to free-surface and a refined mesh generation is adopted to improve calculation stability.

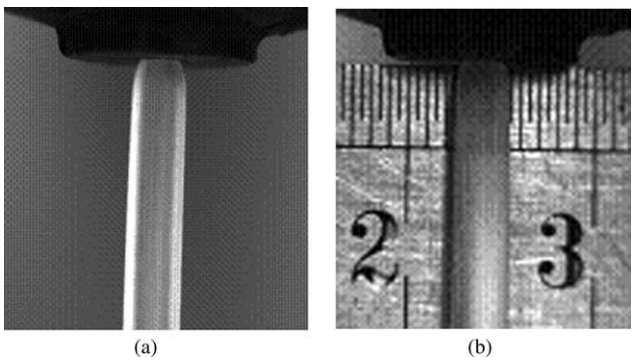

Figure 6 Measurement of extrudate swell.

The swelling ratio S_w as defined in eq. (32) under four different volume flow rates Q_v, Q_v = 8.814e-9 m^3/s, Q_v = 2.061e-8 m^3/s, Q_v = 2.551e-8 m^3/s, and Q_v = 3.6e-8 m^3/s) is investigated both by experimental measurement and numerical simulation as shown in Figure 8.

$$S_w = \frac{A - A_0}{A_0} \times 100\% \tag{32}$$

where A is the area of extrudate cross section when arriving flow balance and A_0 is the area of die lip cross section.

It can be found that the effect of volume flow rate on swelling ratio is not obvious under current shear rate and the simulated results are a little larger than those obtained by experimental measurement. Figure 9 is the comparison of radial dimension of extrudate near the die lip, respectively, obtained by experiment and simulation (Q_v = 8.814e-9 m^3/s). The simulated results are found to be a little larger than those obtained by experimental measurement. The difference between the mathematical model and practical processing conditions, such as the length diameter ratio of extrusion die, the hypothesis of nonslip, and the ignore of gravity, may cause the deviations of simulated results. Besides, the inherent defect of constitutive equation may be another reason to cause the deviation. However, it is still difficult to quantitatively predict the field variables directly through experimental measurement. The proposed numerical simulation technology can be a reasonable alternative for the investigation of complex swell phenomenon like in the LDPE annular extrusion process. It can be adopted to qualitatively and quantitatively predict melts flow patterns and hence to reveal material forming mechanism.

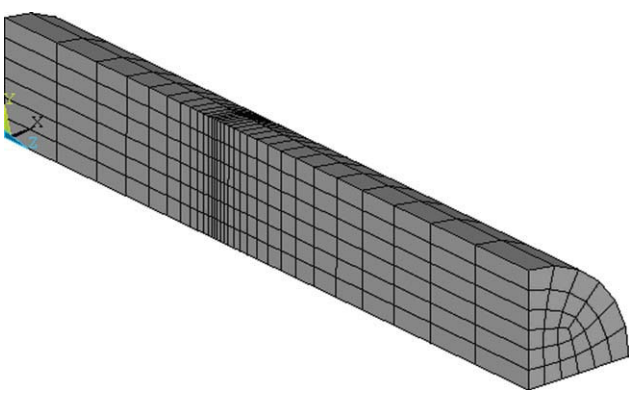

Figure 7 Finite element model of the solved domain. [Color figure can be viewed in the online issue, which is available at www.interscience.wiley.com.]

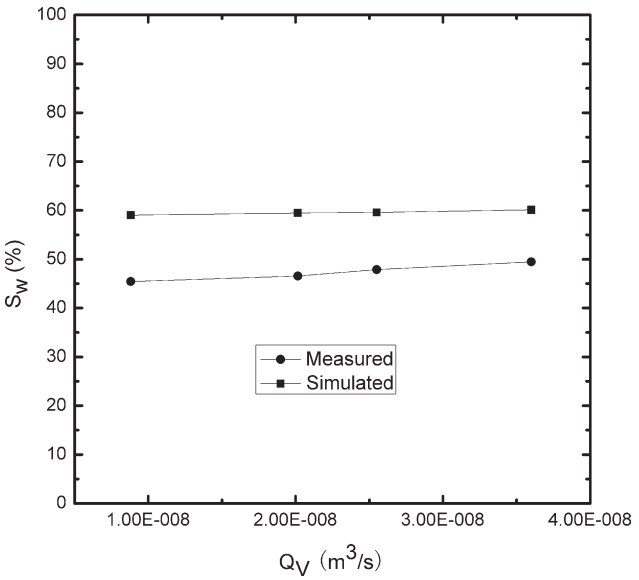

Figure 8 Comparison of swelling ratios under different volume flow rates.

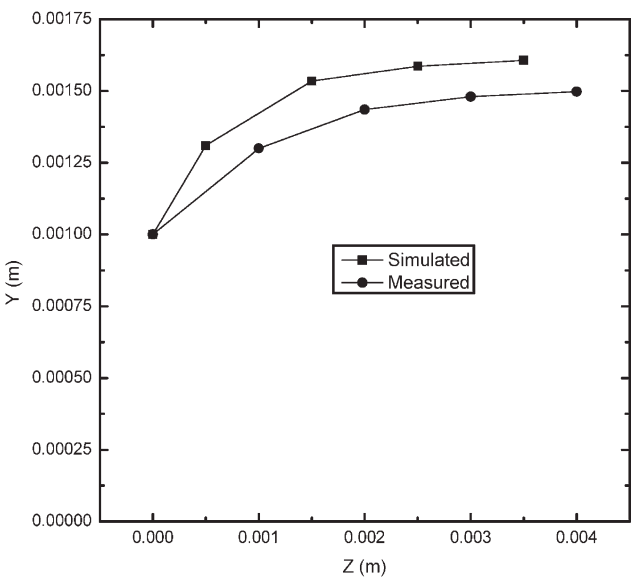

Figure 9 Comparison of swelling dimension (Q_v = 8.814e-9).

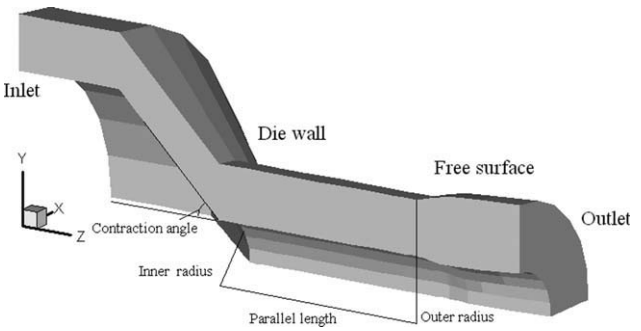

Figure 10 Parameters and boundaries of the annular extrusion die.

MODELING OF ANNULAR EXTRUSION

Geometrical model

The annular extrusion die presented in the study is a typical structure applied in practical polymer processing. A fully developed straight flow is firstly formed in the adapter and then converted to the required shape and dimension by the contraction of the transition zone. A newly oriented flow is thereafter developed in the parallel zone. Polymer melts experience violent shear and extension within the extrusion die and the melts deformation history will affect downstream flow patterns significantly. As for the annular flow of polymer melts, parameters of the extrusion die as shown in Figure 10 are important factors that can influence polymer melts rheological behaviors both within and out of the die.

Boundary conditions

Only when the real boundary conditions being introduced, the calculations of governing equations could reflect practical physical phenomenon. As it is shown in Figure 10, the annular extrudate swell problem has the following characteristic boundaries.

On the inflow boundary, the flow is fully developed and the axial velocity can be imposed as follows on the inlet with radial velocity being set to zero

$$u_z = \frac{2Q_v}{\pi R_o'^2}\left(1 - \frac{r^2}{R_o'^2} + \frac{1-k^2}{1\mathrm{n}\frac{1}{k}} ln\left(\frac{r}{R_o'}\right)\right) \cdot \left[(1-k^4) - \frac{(1-k^2)^2}{ln\frac{1}{k}}\right]^{-1} \quad (33)$$

where $r = \sqrt{x^2 + y^2}$, $k = R_\mathrm{i}'/R_\mathrm{o}'$ is the ratio of inner to outer radius on the inlet face, Q_v is the volume flow rate. The associate inlet stress can be calculated by submitting the velocity profile into eq. (8) along with all of the gradient components in the primary flow direction being set to zero.

On the die wall, the nonslip condition can be imposed on all the velocity components as follows:

$$u_x = u_y = u_z = 0 \quad (34)$$

Because of the vanishing of convective derivatives in the constitutive equation, the stress components can be calculated iteratively in terms of the nonzero components of the velocity gradients.

On the free surface, both force and velocity boundary conditions are specified with neglecting the effects of surface tension. The tangential component and the normal component of the traction force incorporating the velocity normal to the free surface are imposed as follows:

$$F_n = F_t = 0, \quad u_n = 0 \quad (35)$$

On the downstream outflow boundary, the normal traction force is set to zero in the absence of gravity and surface tension with the assumption of fully developed velocity conditions as follows:

$$F_n = 0, \quad u_t = 0 \quad (36)$$

RESULTS AND DISCUSSION

According to the established numerical model and solution algorithm, a 3D viscoelastic flow simulation is conducted to predict the swell phenomenon of LDPE flowing through out of the annular extrusion die under a definite volume flow rate (Q_v = 2.198e-8 m^3/s). A dimensionless Weissenberg number We can be used to characterize the elasticity effects of the viscoelastic flow and it is defined here as follows:

$$\mathrm{We} = \frac{\lambda \overline{u}}{t} \quad (37)$$

where $\overline{u}$ is the mean flow rate in the downstream flow channel and t is the thickness of the outlet cross section. In this study, the numerical investigation is carried out under We = 13.4 and the stable calculations are successfully executed.

Material parameters obtained through the rheological test, as shown in "Material Characterization," are adopted in the numerical calculation to describe the viscoelastic properties of the commercial LDPE. The initial geometric parameters of the annular extrusion die, as shown in Table 2, are adopted. The flow patterns and swell phenomenon of polymer melts flowing through out of the annular extrusion die with different die parameters, including the die contraction angle α, the radio of parallel length to inner radius L/R_i, and the ratio of outer to inner radius R_o/R_i are obtained by the numerical simulation.

TABLE II
Geometric Parameters (unit : m)

Geometric parameter	Value
Outer radius of the inlet cross section	0.004
Inner radius of the inlet cross section	0.003
Length of the adapter	0.002
Contraction angle (α)	45°
Length of the parallel zone (L)	0.004
Outer radius of the outlet cross-section (R_o)	0.002
Inner radius of the outlet cross-section (R_i)	0.001
Length of the free flow zone	0.002

The essential flow characteristics of polymer melts within the annular flow field are further investigated by the assessments of flow velocity and flow stress in the study.

Mesh dependency

The effects of mesh refinements on the numerical results and the convergence of the numerical scheme is firstly performed in the study and three mesh division schemes are carried out by means of mapping mesh generation technology as shown in Figure 11. The main characteristics of three mesh divisions including the number of nodes, elements and the degree of freedoms (DOF(u) and DOF(S)) are listed as in Table 3.

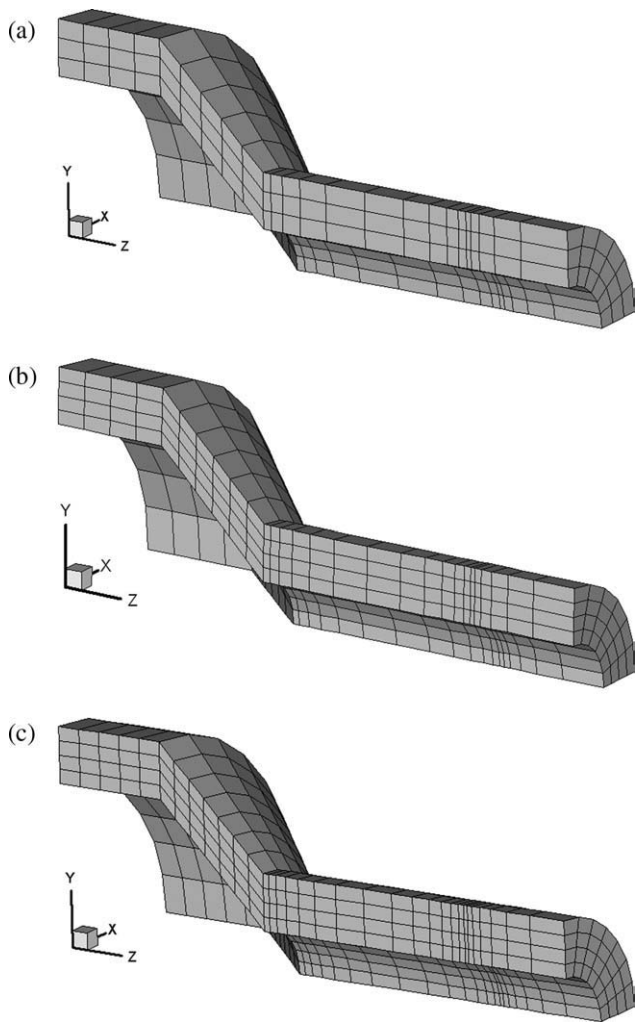

Figure 11 Finite element model of the flow channel: (a) M1; (b) M2; and (c) M3.

TABLE III
Mesh Characteristics

	Mesh M1	Mesh M2	Mesh M3
Elements	432	672	924
Nodes	700	1015	1360
DOF(u)	2100	3045	4080
DOF(S)	4200	6090	8160

Figure 12 is the comparison of extrudate dimension, respectively, predicted with three meshes for the viscoelastic flow of polymer melts flowing through out of the die channel ($\alpha = 45°$, $L/R_i = 4.0$, $R_o/R_i = 2.0$). A similar dimension of extrudate with different mesh divisions is found. Whereas, the coarse mesh M1 leads to a smaller swell of the outer radius. Almost the same predictions are found for the more refined mesh M2 and M3. Considering the sufficient accuracy and computationally cost-effective, we accept mesh M2 as our base mesh and all the results to be given below are computed with the mesh division scheme M2 unless otherwise stated.

Extrudate cross-sectional swell

As it is known that the contraction angle is an important structure parameter for the extrusion die design. In this study, a variable die contraction angle with definite $L/R_i = 4.0$ and $R_o/R_i = 2.0$ is firstly employed. The numerical prediction of polymer

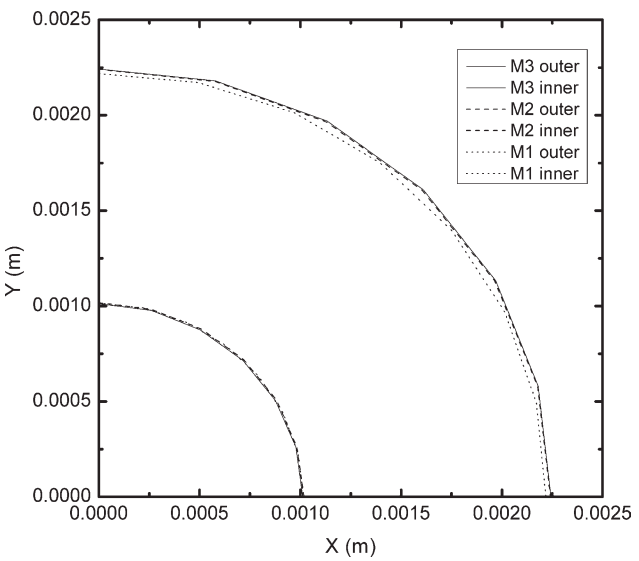

Figure 12 Comparison of extrudate cross-sectional dimension with different mesh divisions ($\alpha = 45°$, $L/R_i = 4.0$, and $R_o/R_i = 2.0$).

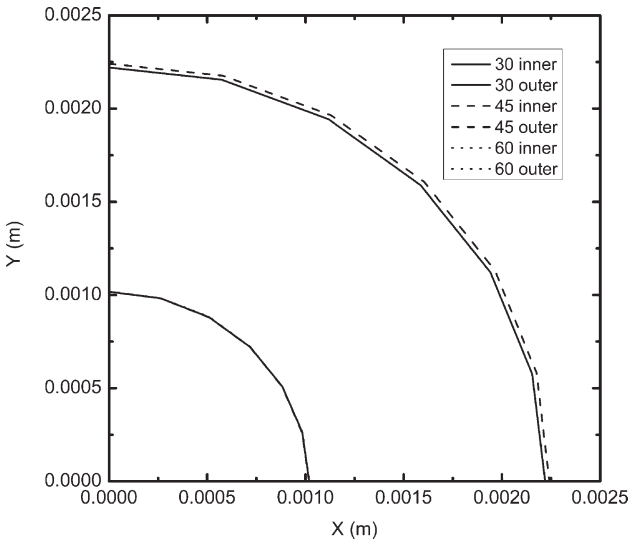

Figure 13 Comparison of extrudate cross-sectional dimension with different die contraction angles (L/R_i = 4.0 and $R_o/R_i = 2.0$).

viscoelastic flow through out of annular extrusion die with different die contraction angles α (α = 30°, α = 45°, and α = 60°) is conducted to quantify the effects of die contraction angle upon the annular extrudate swell phenomenon.

Figure 13 shows the comparison of extrudate cross-sectional dimension with different die contraction angles α (α = 30°, α = 45°, and α = 60°) under definite $L/R_i = 4.0$ and $R_o/R_i = 2.0$. It can be found that both shape and dimension of the extrudate cross section are similar to each other though different die contraction angle is adopted. That is to say, the variation of die contraction angle has little effect on the annular extrudate swell. While, the extrudate shape and dimension change a lot along the flow path out of the die lip. Figure 14 shows the variation of the extrudate cross-sectional dimension on different cross sections ($z = 0.008204$ m, $z = 0.009215$ m, and $z = 0.01$ m) out of 45° contraction die. It can be found that the inner radius of the extrudate firstly expands and then shrinks a little, whereas the outer radius of the extrudate keeps expanding along the melts flow path. As for the extrudate cross-sectional dimension, it keeps increasing until the flow balance is arrived and the extrudate swell ratio as defined in eq. (32) are, respectively, 9.89%, 29.85%, and 32.57% on the three different cross sections.

Besides the die contraction angle, the ratio of parallel length to inner radius is another important die parameter that influences the annular flow pattern and extrudate swell phenomenon. Figure 15 shows the comparison of extrudate cross-sectional dimension with different ratios of parallel length to inner radius L/R_i ($L/R_i = 2.0$, $L/R_i = 4.0$, and $L/R_i = 8.0$) under definite α = 45° and $R_o/R_i = 2.0$. It can be found that the swell ratio decreases from 34.75% to 23.82% with the ratio of parallel length to inner radius increasing from 1 : 1 to 8 : 1. That is to say, the increase of parallel length can help to reduce the swell effects in the polymer processing.

As for the LDPE annular extrusion process, the annular characteristic of the extrusion die can be defined by the ratio of outer to inner radius R_o/R_i which is also an important die parameter besides of the die contraction angle α and the ratio of parallel length to inner radius L/R_i. Figure 16 shows the comparison of extrudate cross-sectional dimension with different ratios of outer to inner radius R_o/R_i ($R_o/R_i = 1.25$, $R_o/R_i = 1.5$, $R_o/R_i = 1.75$, and $R_o/R_i = 2.0$) under definite α = 45° and $L/R_i = 4.0$. It can be found that the swell ratio keeps increasing with

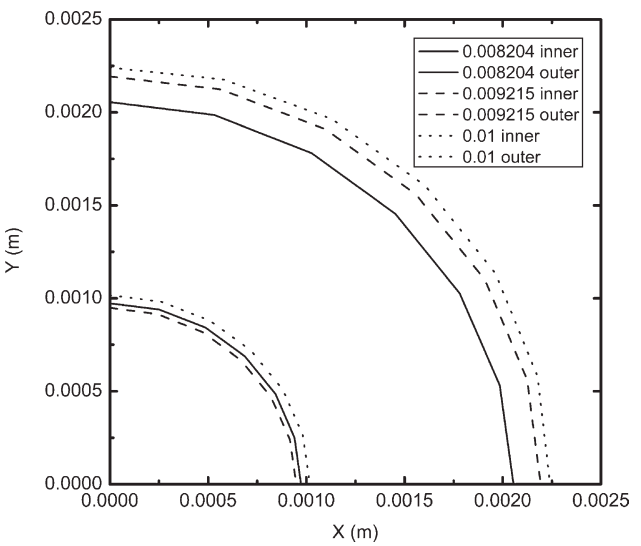

Figure 14 Variation of extrudate cross-sectional dimension out of 45° contraction die ($L/R_i = 4.0$ and $R_o/R_i = 2.0$).

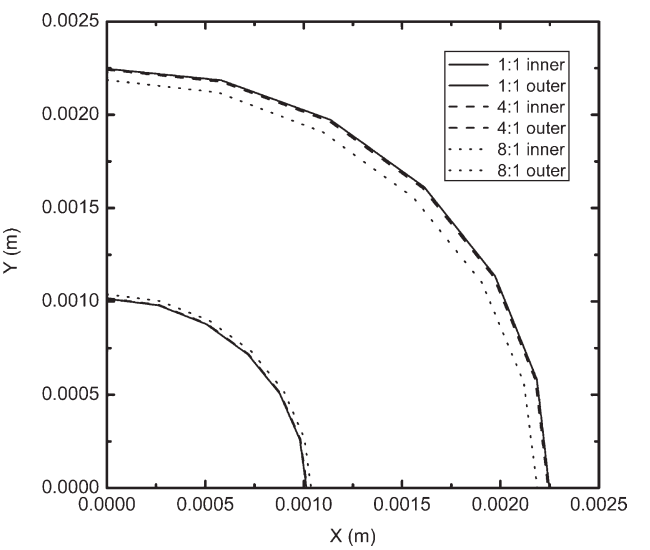

Figure 15 Comparison of extrudate cross-sectional dimension with different ratios of parallel length to inner radius (α = 45° and $R_o/R_i = 2.0$).

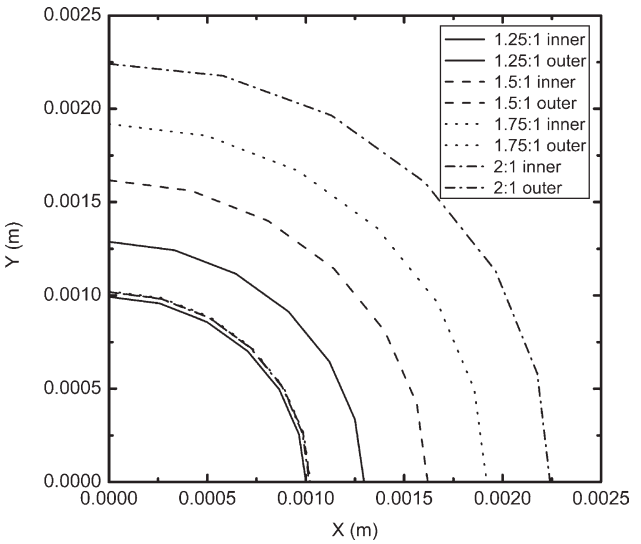

Figure 16 Comparison of extrudate cross-sectional dimension with different ratios of outer to inner radius ($\alpha = 45^\circ$ and $L/R_i = 4.0$).

the increase of the ratio of outer to inner radius as shown in Figure 17. This is because the larger the ratio of outer to inner radius R_o/R_i is, the relative smaller parallel length L will be achieved. The stress cannot be well released if a larger ratio of outer to inner radius is adopted and hence lead to a larger swell of the extrudate. This conclusion can also improve that relative longer parallel length help to release stress and hence reduce the swell ratio.

Distribution of flow velocity

The whole flow patterns of polymer melts within and out of the extrusion die can be fully understood by the prediction of flow velocity distribution. Figures 18–20, respectively, show the comparison of radial velocity u_y and axial velocity u_z of polymer melts along the flow field when the flow balance is achieved with different die contraction angles α, different ratios of parallel length to inner radius L/R_i, and different ratios of outer to inner radius R_o/R_i. Although the variation of die parameters influences the flow field variables in magnitude, the whole flow patterns of polymer melts are similar to each other. The upstream flow velocity has a concentric distribution in the adapter and the flow of polymer melts is relatively faster along the flow channel centerline. The flow velocity keeps increasing when polymer melts flowing through the transition zone and the maximum flow velocity occurs near the joint of transition zone to parallel zone. After the developing flow of polymer melts in the parallel zone, the radial velocity u_y abruptly increases when approaching to the flow channel outlet and another maximum value is achieved both near the inner wall of die lip and near the outer wall of die lip. Meanwhile, the radial velocity u_y decreases to be zero near the flow channel centerline and the axial velocity u_z also decreases rapidly to be redistributed in the downstream flow field. It can be concluded from the analysis of the flow velocity that the redistribution of flow velocity can be an important reason to cause the phenomenon of LDPE annular extrudate swell.

Figure 18 shows the comparison of velocity distribution with different die contraction angles α ($\alpha = 30^\circ$, $\alpha = 45^\circ$, and $\alpha = 60^\circ$) under definite $L/R_i = 4.0$ and $R_o/R_i = 2.0$. It can be found that the maximum axial flow velocity u_z appears near the joint of transition zone to parallel zone and its values increases with the increase of die contraction angle. The maximum radial flow velocity u_y appears near the flow channel outlet, but its value is not appreciably affected by the variation of die contraction angle. This is just in accordance with the illustration in "Extrudate cross-sectional swell" that the variation of die contraction angle has little effect on the annular extrudate swell. Figure 19 shows the comparison of velocity distribution with different ratios of parallel length to inner radius L/R_i ($L/R_i = 2.0$, $L/R_i = 4.0$, and $L/R_i = 8.0$) under definite $\alpha = 45^\circ$ and $R_o/R_i = 2.0$. We can find that the increase of parallel length have little effect on the whole distribution of flow velocity. While, the value of radial flow velocity u_i near the flow channel outlet keeps decreasing with the increase of the parallel length L. This is just in accordance with the conclusion that longer parallel length help to release stress and hence reduce the swell ratio as illustrated in Extrudate cross-sectional swell. Figure 20 shows the comparison of velocity distribution with different ratios of outer to inner radius R_o/R_i ($R_o/R_i = 1.25$, $R_o/R_i = 1.5$, $R_o/R_i = 1.75$,

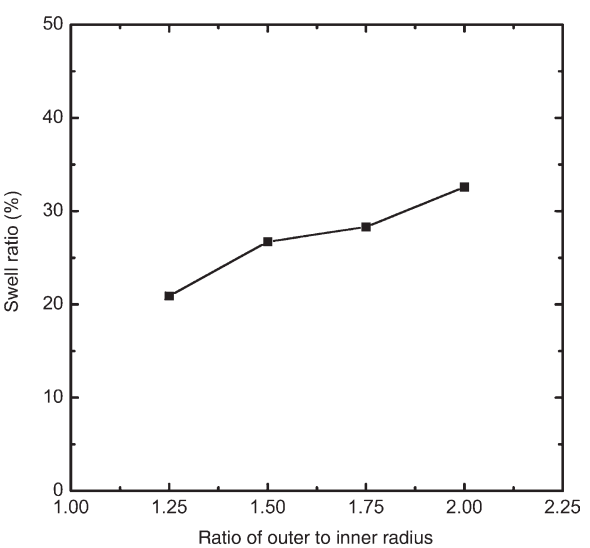

Figure 17 Comparison of swell ratio with different ratios of outer radius to inner radius ($\alpha = 45^\circ$ and $L/R_i = 4.0$).

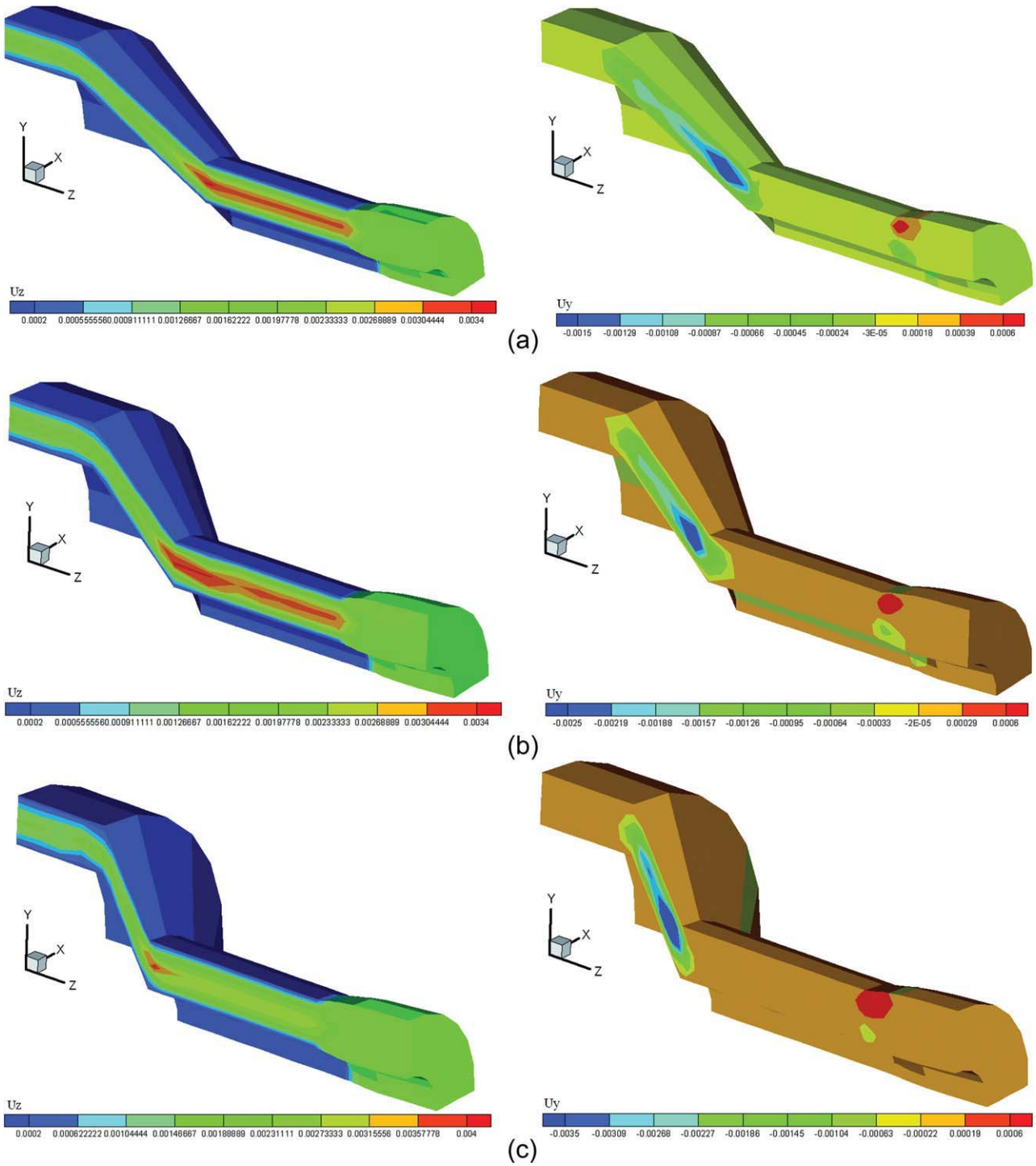

Figure 18 Comparison of velocity distribution with different die contraction angles ($L/R_y = 4.0$, $R_o/R_y = 2.0$): (a) $\alpha = 30°$; (b) $\alpha = 45°$; and (c) $\alpha = 60°$. [Color figure can be viewed in the online issue, which is available at www.interscience.wiley.com.]

and $R_o/R_i = 2.0$) under definite $\alpha = 45°$ and $L/R_i = 4.0$. As it is shown that the smaller the ratio of outer to inner radius is designed to be, the larger the maximum flow velocity near the joint of transition zone to parallel zone will be. Meanwhile, the radial flow velocity u_y near the flow channel outlet keeps increasing with the increase of the ratio of outer to inner radius. That is why we find that the swell ratio keeps increasing with the increase of ratio of outer to inner radius as illustrated in "Extrudate cross-sectional swell".

Distribution of flow stress

When flowing through the annular extrusion die, polymer melts will experience strong shear and extension. The resulting melts deformation history

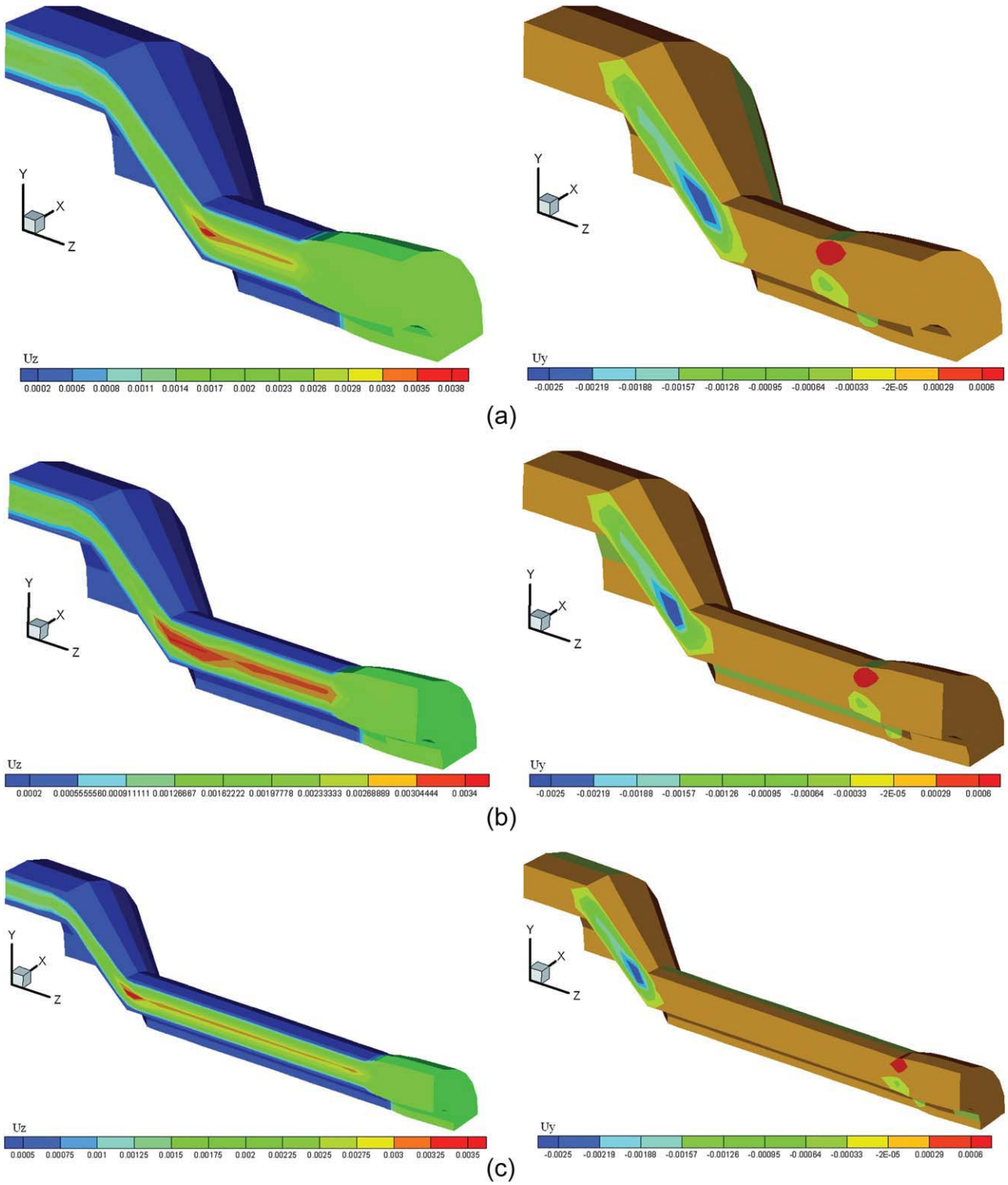

Figure 19 Comparison of velocity distribution with different ratios of parallel length to inner radius ($\alpha = 45°$, $R_o/R_i = 2.0$): (a) $L/R_i = 2.0$; (b) $L/R_i = 4.0$; and (c) $L/R_i = 8.0$. [Color figure can be viewed in the online issue, which is available at www.interscience.wiley.com.]

can be predicted by the investigation of flow stress distribution. Figures 21–23, respectively, show the comparison of shear stress S_{yz} and normal stress S_{zz} along the flow field with different die contraction angles α, different ratios of parallel length to inner radius L/R_i, and different ratios of outer to inner radius R_o/R_i. It can be found that the shear flow behavior of polymer melts dominated in the adapter. When entering the transition zone, the extensional flow of polymer melts is enhanced and the normal

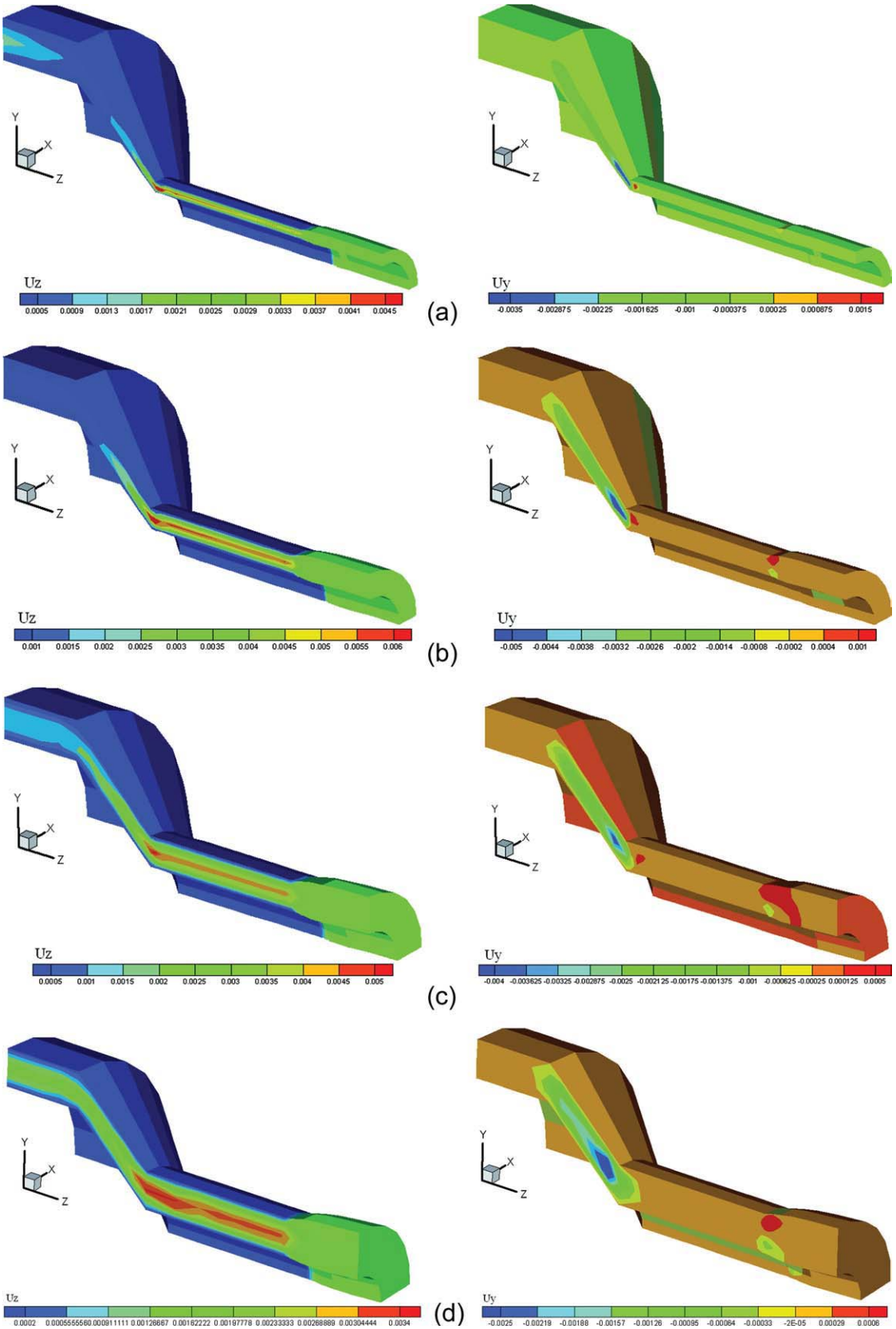

Figure 20 Comparison of velocity distribution with different ratios of outer to inner radius ($\alpha = 45^\circ$, $L/R_i = 4.0$): (a) $R_o/R_i = 1.25$; (b) $R_o/R_i = 1.5$; (c) $R_o/R_i = 1.75$; and (d) $R_o/R_i = 2.0$. [Color figure can be viewed in the online issue, which is available at www.interscience.wiley.com.]

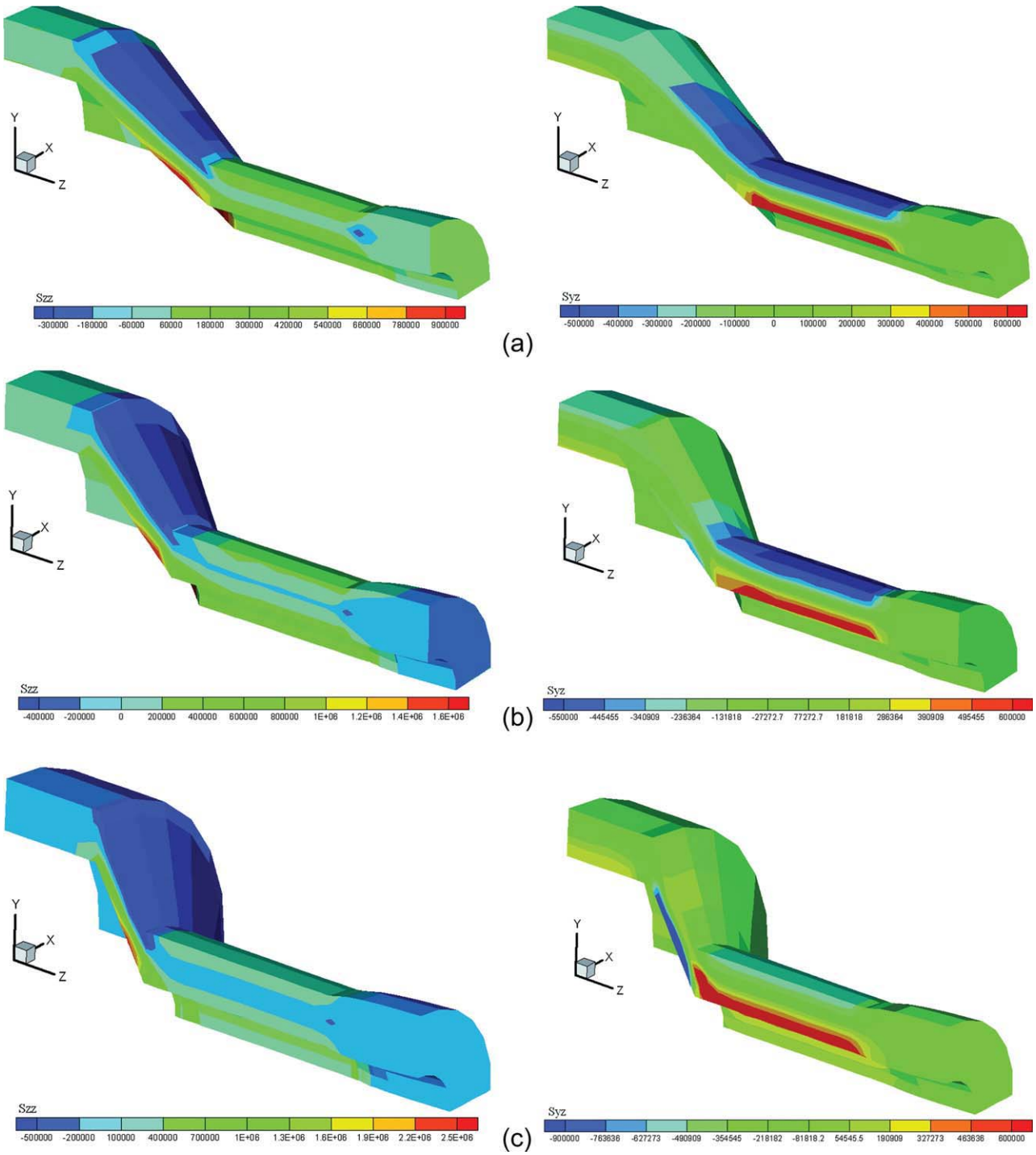

Figure 21 Comparison of stress distribution with different die contraction angles ($L/R_i = 4.0$, $R_o/R_i = 2.0$): (a) $\alpha = 30°$; (b) $\alpha = 45°$; and (c) $\alpha = 60°$. [Color figure can be viewed in the online issue, which is available at www.interscience.wiley.com.]

stress increases rapidly. While in the following parallel zone, the shear flow is enhanced and extensional flow is weakened. Polymer melts experience stronger effects of axial shear and radial extension near the die wall than that experienced along the centerline in the parallel flow field. The effects of stress keep developing until the melts flow approaches to the die lip where the distribution of shear stress abruptly changes. The original axial shear turns to be radial shear and its maximum value increases a lot. Meanwhile, extension effect on the polymer melts caused by normal stress is greatly improved. The maximum normal stress appears both near the inner wall of die lip and near the outer

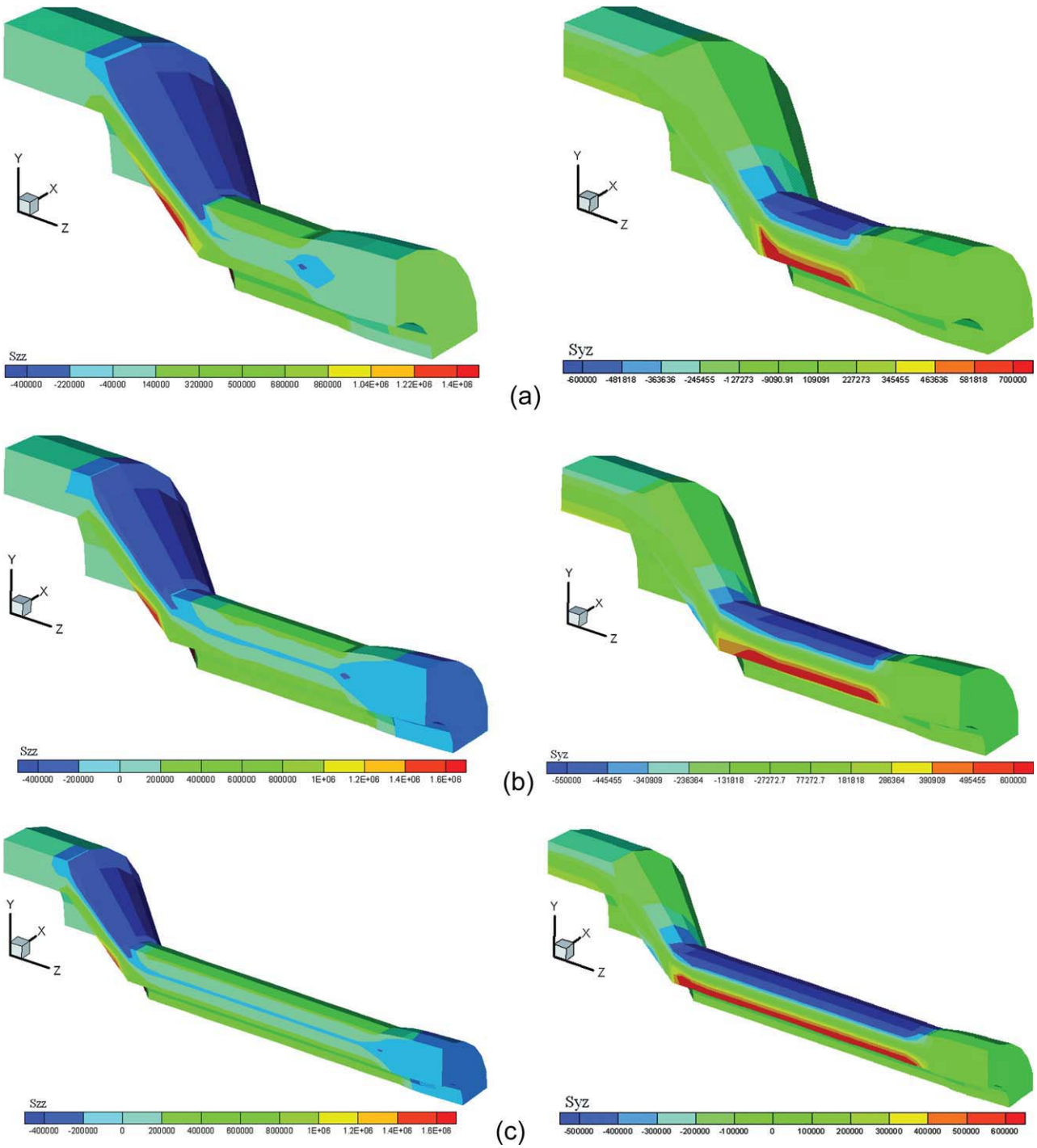

Figure 22 Comparison of stress distribution with different ratios of parallel length to inner radius ($\alpha = 45°$, $R_o/R_i = 2.0$): (a) $L/R_i = 2.0$; (b) $L/R_i = 4.0$; and (c) $L/R_i = 8.0$. [Color figure can be viewed in the online issue, which is available at www.interscience.wiley.com.]

wall of die lip, but it decreases rapidly near the centerline of die lip. In the downstream flow field, the stress is well distributed and the melts flow is steady and smooth. So, the swelling phenomenon accompanies with complex release of flow stress and it greatly influences the rheological behaviors of polymer melts.

Figure 21 shows the comparison of stress distribution with different die contraction angles α ($\alpha = 30°$, $\alpha = 45°$, and $\alpha = 60°$) under definite $L/R_i = 4.0$ and $R_o/R_i = 2.0$. It can be found that the maximum normal stress S_{zz} occurs in the transition zone and its value increases with the increase of die contraction angle. The maximum shear stress S_{yz} occurs in the

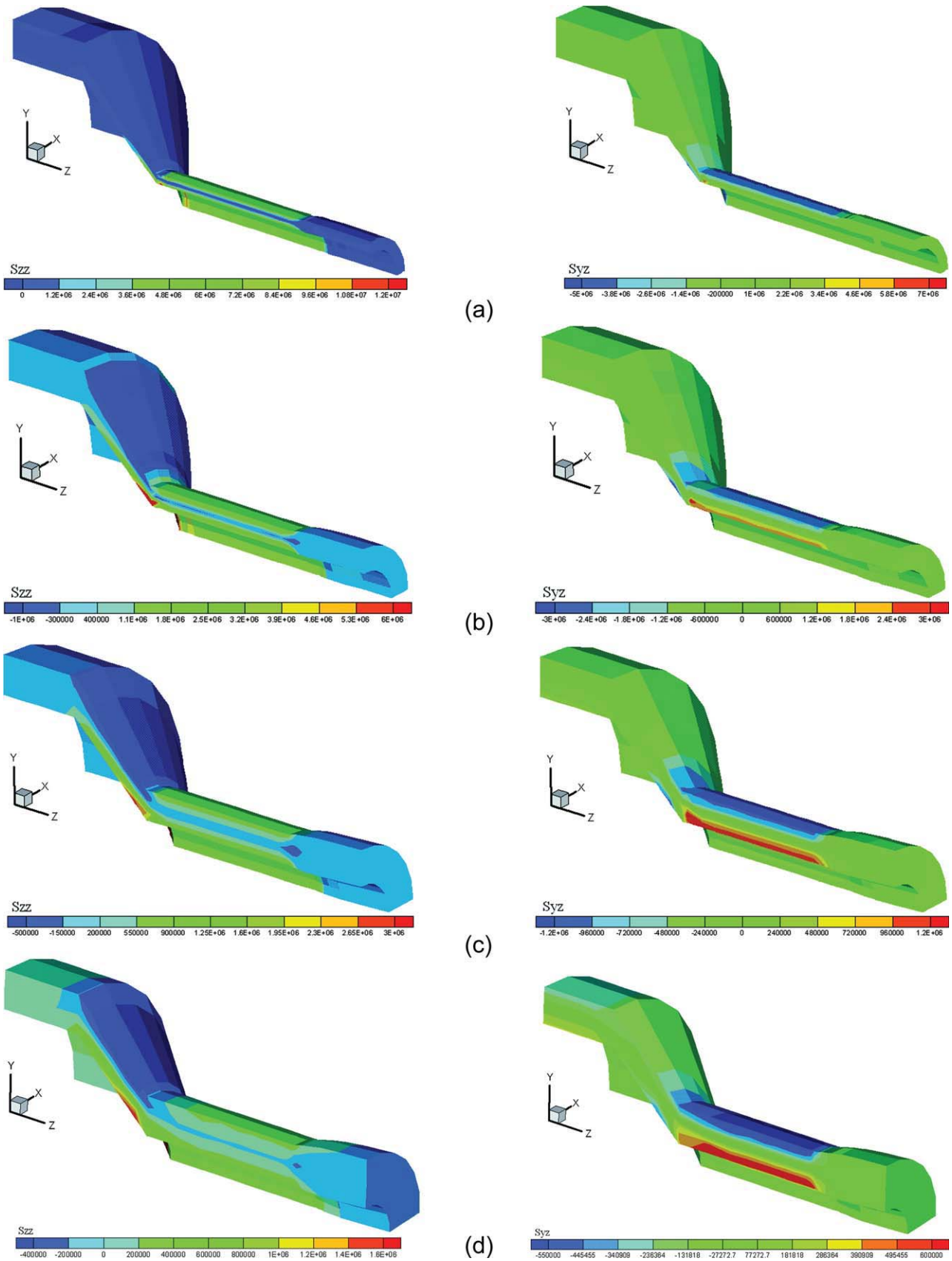

Figure 23 Comparison of stress distribution with different ratios of outer to inner radius ($\alpha = 45^\circ$, $L/R_i = 4.0$): (a) $R_o/R_i = 1.25$; (b) $R_o/R_i = 1.5$; (c) $R_o/R_i = 1.75$; and (d) $R_o/R_i = 2.0$. [Color figure can be viewed in the online issue, which is available at www.interscience.wiley.com.]

parallel zone and its value also increases with the contraction angle increasing. So with the increase of die contraction angle, polymer melts experience much stronger shear and extension especially near the joint of transition zone to parallel zone. That is to say, the increase of die contraction angle may cause instable flow problem and hence affect the final products performance. As it is illustrated in "Extrudate cross-sectional swell" that the variation of die contraction angle has little effect on the annular extrudate swell, so a small die contraction angle is recommended in practical die design to ensure a stable extrusion flow. Figure 22 shows the comparison of stress distribution with different ratios of parallel length to inner radius L/R_i ($L/R_i = 2.0$, $L/R_i = 4.0$, and $L/R_i = 8.0$) under definite $\alpha = 45^\circ$ and $R_o/R_i = 2.0$. It can be found that the variation of parallel length has little effect on the value of flow stress. While, a relative well distribution of flow stress is achieved near the flow channel outlet with the increase of parallel length. That is why a larger ratio of parallel length to inner radius may reduce the annular extrudate swell as illustrated in "Extrudate cross-sectional swell". So, longer parallel length is recommended in practical die design on condition that the extrusion pressure can afford to. Figure 23 shows the comparison of stress distribution with different ratios of outer to inner radius R_o/R_i ($R_o/R_i = 1.25$, $R_o/R_i = 1.5$, $R_o/R_i = 1.75$, and $R_o/R_i = 2.0$) under definite $\alpha = 45^\circ$ and $L/R_i = 4.0$. It can be found that the variations of ratio of outer to inner radius can greatly influence the polymer melts flow pattern. As the ratio of outer to inner radius decreases from 2 : 1 to 1.5 : 1, the maximum shear stress S_{yz} and normal stress S_{zz} both increase about four times. When the ratio of outer to inner radius decreases to be 1.25 : 1, the maximum values of shear stress S_{yz} and normal stress S_{zz} increase even to exceed the critical stress value that will inevitably lead to instable flow problems. So, the decrease of the ratio of outer to inner radius can in one hand decrease the swell ratio of extrudate, but in the other hand increase the occurrence probability of instable flow problems and hence cause the quality problems of the extrudate. So, a ratio of outer to inner radius between 2 : 1 and 1.5 : 1 is recommended in practical die design of annular extrusion.

CONCLUSIONS

The swell behavior of polymer melts flow caused by material viscoelastic property in the polymer processing can greatly affect the dimension and precision of the extrudate. The swell phenomenon of LDPE flowing through annular extrusion die was predicted by the numerical simulation technology and the effects of die parameters were investigated in detail. A comprehensive understanding on the LDPE annular extrudate swell phenomenon was obtained.

1. The viscoelastic behavior of a commercial LDPE was depicted by PTT constitutive model and the rheological parameters was obtained by fitting the distributions of material functions detected in simple flows executed on a strain-controlled rheometer.
2. The mathematical model of swell phenomenon of polymer melts flowing through out of annular extrusion die was established. A penalty finite element based on DEVSS/SU method has been implemented for the prediction of the swell phenomenon of LDPE annular extrusion. The streamface-streamline method was employed to update the free surface. Stable calculation was achieved by using a decoupled scheme.
3. The influences of annular die parameters including die contraction angle α, the ratio of parallel length to inner radius L/R_i, and the ratio of outer to inner radius R_o/R_i on both the extrudate swell ratio and the polymer melts flow patterns were discussed in detail. It was found that the die contraction angle have little effect on the swell ratio, whereas the increase of die contraction angle may cause instable flow near the joint of transition zone to parallel zone. The increase of the ratio of parallel length to inner radius can help to release the flow stress and hence to decrease the extrudate swell ratio. It was also found that the decrease of the ratio of outer to inner radius may cause the decrease of the extrudate swell ratio for the reason that a relative longer parallel length can be obtained. According to the results of the numerical investigation, an optimal design of the annular extrusion die may be achieved by using smaller die contraction angle, longer parallel length, and intermediate ratio of outer to inner radius.
4. The distributions of flow velocity and flow stress of LDPE melts within the annular extrusion die were obtained by using finite element simulation. The characteristics of flow velocity and flow stress were investigated and it was found that both the redistribution of flow velocity and the release of flow stress should be the reasons for the swell phenomenon.

It is a preliminary investigation on the effect of die geometry on the swell phenomenon of polymer melts flowing through annular extrusion die. A further consideration on the optimization for practical extrusion die design will be introduced in the future study.

NOMENCLATURE

u	velocity vector
p	hydrostatic pressure
S	extra stress tensor
d	strain rate tensor
τ	polymer-contribution stress
η_v	newtonian-contribution viscosity
β	retardation ratio
η_p	polymer-contribution viscosity
η_t	total viscosity
λ	relaxation time
$\overline{\eta}$	reference viscosity
ε	elasticity parameter
ξ	slip parameter
λ_p	penalty factor
δ_u, δ_τ, δ_x, δ_y	convergent criterion
ω	angular frequency
G'	storage modulus
G''	loss modulus
S_w	swell ratio

References

1. Lodge, A. S. Elastic Liquids; Academic Press: London, 1964.
2. Tanner, R. I. J Polym Sci Part A: Polym Phys 1970, 8, 2067.
3. Nickell, R. E.; Tanner, R. I.; Caswell, B. J Fluid Mech 1974, 65, 189.
4. Chang, P. W.; Patten, T. W.; Finlayson, B. A. Comput Fluids 1979, 7, 285.
5. Caswell, B.; Viriyayuthakorn, M. J Nonnewtonian Fluid Mech 1983, 12, 13.
6. Bush, M. B.; Milthorpe, J. F.; Tanner, R. I. J Nonnewtonian Fluid Mech 1984, 16, 37.
7. Phan-Thien, N.; Tanner, R. I. J Nonnewtonian Fluid Mech 1977, 2, 353.
8. Mitsoulis, E. Comput Methods Appl Mech Eng 1999, 180, 333.
9. Huilgol, R. R.; Phan-Thien, N. Fluids Mechanics of Viscoelasticity; Elsevier: Amsterdam, 1997.
10. Chung, T. J. Finite Element Analysis in Fluid Dynamics; McGraw-Hill: New York, 1978.
11. Larson, R. G. Constitutive Equations for Polymer Melts and Solutions; Butterworths: Boston, 1988.
12. Mu, Y.; Zhao, G. Q.; Qin, S. X.; Chen, A. B. Polym Adv Technol 2007, 18, 1004.
13. Shiojima, T. Int J Numerical Methods Eng 1988, 25, 43.
14. Guénette, R.; Fortin, M. J Nonnewtonian Fluid Mech 1995, 60, 27.
15. Marchal, J. M.; Crochet, M. J. J Nonnewtonian Fluid Mech 1987, 26, 77.